September 2019 Antarctic sudden stratospheric warming: quasi-6-day wave burst and ionospheric effects

Y. Yamazaki[1], V. Matthias[2], Y. Miyoshi[3], C. Stolle[1,4], T. Siddiqui[1], G. Kervalishvili[1], J. Laštovička[5], M. Kozubek[5], W. Ward[6], D. R. Themens[6], S. Kristoffersen[6], P. Alken[7,8]

[1]GFZ German Research Centre for Geosciences, Potsdam, Germany
[2]Potsdam Institute for Climate Impact Research, Potsdam, Germany
[3]Department of Earth and Planetary Sciences, Kyushu University, Fukuoka, Japan
[4]Faculty of Science, University of Potsdam, Potsdam, Germany
[5]Institute of Atmospheric Physics CAS, Prague, Czech Republic
[6]Department of Physics, University of New Brunswick, Fredericton, New Brunswick, Canada
[7]Cooperative Institute for Research in Environmental Sciences, University of Colorado Boulder, Boulder, CO, USA
[8]National Centers for Environmental Information, NOAA, Boulder, CO, USA

Key Points:

- An Antarctic sudden stratospheric warming (SSW) occurred in September 2019
- Swarm observations reveal prominent 6-day variations in the dayside low-latitude ionosphere
- A burst of quasi-6-day wave activity is observed in the middle atmosphere during the SSW

Corresponding author: Yosuke Yamazaki, yamazaki@gfz-potsdam.de

Abstract

An exceptionally strong stationary planetary wave with Zonal Wavenumber 1 led to a sudden stratospheric warming (SSW) in the Southern Hemisphere in September 2019. Ionospheric data from ESA's Swarm satellite constellation mission reveal prominent 6-day variations in the dayside low-latitude region at this time, which can be attributed to forcing from the middle atmosphere by the Rossby normal mode "quasi-6-day wave" (Q6DW). Geopotential height measurements by the Microwave Limb Sounder aboard NASA's Aura satellite show a burst of Q6DW activity in the mesosphere and lower thermosphere during the SSW, which is one of the strongest in the record. The Q6DW is apparently generated in the polar stratosphere at 30–40 km, where the atmosphere is unstable due to strong vertical wind shear connected with planetary-wave breaking. These results suggest that an Antarctic SSW can lead to ionospheric variability through wave forcing from the middle atmosphere.

1 Introduction

A sudden stratospheric warming (SSW) is a large-scale meteorological phenomenon in the winter stratosphere, which involves a rapid rise in the polar temperature by a few tens of K in several days (Andrews, Leovy, & Holton, 1987; Labitzke & Van Loon, 1999). An SSW is triggered by an injection of stationary planetary waves (PWs) from the troposphere, which are driven by topography and land-sea temperature contrasts. PW breaking in the middle atmosphere leads to an acceleration of the zonal mean flow and changes the mean meridional circulation (Matsuno, 1971). Dynamical effects of PW breaking during SSWs are not limited in the stratosphere but are also well extended into the mesosphere and lower thermosphere (Chandran, Collins, & Harvey, 2014).

According to the definition by the World Meteorological Organization (McInturff, 1978), a "minor" SSW occurs when a large temperature increase is observed in the winter polar stratosphere, at least by 25 K in a week or less. The event is called "major" if the reversal of the zonal mean flow from eastward to westward occurs poleward of 60° latitude at 10 hPa (32 km) or below, along with the reversal of the meridional temperature gradient. The average number of major SSWs is ∼0.6 per winter in the Northern Hemisphere (NH) (Butler et al., 2015; Charlton & Polvani, 2007). In the Southern Hemisphere (SH), the occurrence of an SSW, whether major or minor, is not as frequent as in the NH because of weaker PW forcing due to smaller topographical differences and land-sea contrasts. In fact, the September 2002 event (Baldwin, Hirooka, O'Neill, & Yoden, 2003; Krüger, Naujokat, & Labitzke, 2005) is the only major SSW observed in the Antarctic.

In the last decade, the aeronomy community has come to the realization that SSWs can be a significant source of ionospheric variability (Chau, Goncharenko, Fejer, & Liu, 2012; Pedatella et al., 2018). In particular, the January 2009 major Arctic SSW, which took place under extremely quiet solar- and geomagnetic-activity conditions, enabled many studies to attribute observed ionospheric perturbations to the SSW (e.g., Chau et al., 2010; Fejer et al., 2010; Goncharenko, Chau, Liu, & Coster, 2010; Goncharenko, Coster, Chau, & Valladares, 2010; Lin et al., 2019; H. Liu et al., 2011; Nayak & Yiğit, 2019; Oyama et al., 2014; Pancheva & Mukhtarov, 2011; Patra, Pavan Chaitanya, Sripathi, & Alex, 2014; Pedatella & Forbes, 2010; Rodrigues, Crowley, Azeem, & Heelis, 2011; Yadav et al., 2017; Yue et al., 2010). Most studies concentrated on the dayside low-latitude re-

gion, where the ionospheric response to the SSW was most pronounced. Modeling studies have suggested that atmospheric tides played an important role in driving ionospheric variability during the January 2009 SSW (Fang et al., 2012; Fuller-Rowell et al., 2011; Jin et al., 2012; Pedatella et al., 2014; Pedatella & Maute, 2015; Sassi, Liu, Ma, & Garcia, 2013; Wang et al., 2014). Tidal waves at altitudes of the ionospheric E region (95–150 km) are, in large part, from the middle atmosphere, and their amplitudes and phases can change in response to an SSW (Stening, Forbes, Hagan, & Richmond, 1997). Among different tidal modes, the semidiurnal lunar tide shows a particularly strong and consistent response to SSWs (Chau, Hoffmann, Pedatella, Matthias, & Stober, 2015; Zhang & Forbes, 2014). Forbes and Zhang (2012) argued that the large semidiurnal lunar tide observed during the January 2009 SSW can arise from resonant amplification associated with the atmospheric Pekeris mode. Enhanced lunar tidal perturbations in the equatorial ionosphere have been reported for a number of SSW events (Fejer, Tracy, Olson, & Chau, 2011; J. Liu, Zhang, Hao, & Xiao, 2019; Park, Lühr, Kunze, Fejer, & Min, 2012; Siddiqui et al., 2018; Siddiqui, Stolle, Lühr, & Matzka, 2015; Yamazaki, Richmond, & Yumoto, 2012).

As mentioned earlier, SSWs rarely occur in the SH, and the ionospheric response to Antarctic SSWs has been largely unexplored. The only exception is the study by Olson, Fejer, Stolle, Lühr, and Chau (2013), which examined ionospheric variability during the September 2002 major Antarctic SSW. Although Olson et al. (2013) observed multi-day variations in the equatorial ionosphere, their association with the SSW remained somewhat uncertain because of high geomagnetic activity during the event. The main objective of this study is to present observations from the ionosphere and middle atmosphere during the recent Antarctic SSW event in September 2019 and note the presence of unusually strong traveling PW activity throughout the atmosphere and ionosphere at this time.

2 Results and Discussion

2.1 September 2019 sudden stratospheric warming

Figure 1 gives an overview of the September 2019 SSW. The polar temperature at 10 hPa, obtained from the MERRA-2 reanalysis (Gelaro et al., 2017), shows a rapid increase from 207.7 K on 5 September to 258.5 K on 11 September 2019 (ΔT=50.8 K/week)

(Figure 1a). This is the largest increase in the Antarctic polar temperature per week in the entire MERRA-2 data set starting from January 1980. The maximum temperature rise during the September 2002 major SSW was ΔT=38.5 K/week. Figure 1b presents the vertical structure of the zonal mean zonal wind at 60°S, as derived from geopotential height (GPH) measurements by the Aura Microwave Limb Sounder (MLS) (Schwartz et al., 2008; Waters et al., 2006). It can be seen that the eastward zonal mean wind first reversed in the upper mesosphere on 2 September 2019, and in the subsequent days, the region of the wind reversal descended to lower layers, reaching 40 km on 18 September 2019. Since the wind reversal did not reach the 10 hPa level (∼32 km), the event is categorized as a minor warming. Figure 1c shows that there was an enhancement in the amplitude of the stationary PW with Zonal Wavenumber (ZW) 1 during 14–20 August 2019 and during 28 August–5 September 2019. In both cases, the amplitude attained the largest recorded by Aura/MLS since August 2004. The former event can contribute to the SSW by weakening the zonal mean flow, which is often referred to as preconditioning (e.g., Cámara et al., 2017; Limpasuvan, Thompson, & Hartmann, 2004; McIntyre, 1982). Forcing due to PW breaking during the latter event is the likely cause of the zonal wind reversal in the middle atmosphere, and hence the SSW. No similar enhancement is found in the amplitude of the stationary PW with ZW2.

As a brief summary, the September 2019 Antarctic SSW was a minor warming but it involved an exceptionally strong stationary PW with ZW1 and a large temperature rise. Furthermore, the event took place during the minimum phase of the solar cycle, similar to the January 2009 SSW, and as will be shown later, overall solar and geomagnetic activities were low, which helps identify SSW effects on the ionosphere. Therefore, the September 2019 event provides an excellent (and rare) opportunity to investigate the ionospheric response to an Antarctic SSW, which is not well understood from previous studies.

2.2 Ionospheric observations by Swarm

ESA's Earth observation mission Swarm (Friis-Christensen, Lühr, & Hulot, 2006) involves three identical satellites (A, B and C), equipped with scientific instruments that are suitable for investigating Earth's magnetic field and its source currents (Friis-Christensen, Lühr, Knudsen, & Haagmans, 2008). The three spacecraft were launched into polar orbits on 22 November 2013, and since 17 April 2014, Swarm A and C fly side-by-side at

an altitude of ∼460 km while Swarm B flies at ∼510 km. Figures 2a–2c show the temporal variability of the equatorial electrojet (EEJ) intensity (e.g., Alken et al., 2015), electron density (e.g., Buchert et al., 2015), and total electron content (TEC) (e.g., Park et al., 2017) as observed by Swarm B during 5 September–5 October 2019. The data used here were collected from the descending parts of the orbit in 11:00–14:00 magnetic local time (MLT) (see also Figure 2g). Figures 2h and 2i show that overall solar and geomagnetic activity levels were low during this time interval, which is typical for solar minimum conditions. Moderately high geomagnetic activity was observed during 27 September–1 October 2019, which needs to be taken into account when the ionospheric data are interpreted. Unlike the September 2002 Antarctic SSW, which was examined by Olson et al. (2013), severe geomagnetic activity with Kp>6 was not observed. The low $F_{10.7}$ conditions are preferable for the study of SSW effects on the ionosphere. Modeling studies have shown that the ionospheric response to lower atmospheric forcing would be more pronounced under lower solar flux conditions (Fang, Fuller-Rowell, Wang, Akmaev, & Wu, 2014; H.-L. Liu & Richmond, 2013).

The EEJ is a narrow band of a zonal electric current that flows along the magnetic equator in the dayside E-region ionosphere at 100-115 km altitude (e.g., Yamazaki & Maute, 2017). During geomagnetically quiet periods, day-to-day variations of the EEJ intensity are dominated by the changes in neutral winds at E-region heights associated with atmospheric waves from the lower layers (Yamazaki et al., 2014), and thus are a good indicator of lower-atmospheric influence on the E-region ionosphere. The methods for deriving the EEJ intensity and equatorial zonal electric field (EEF) from Swarm magnetic field measurements are detailed in Alken, Maus, Vigneron, Sirol, and Hulot (2013). Figure 2a reveals that the EEJ variability was dominated by 6-day variations during this period. The westward phase propagation of the EEJ intensity perturbations with ZW1 can also be seen. Similar spatial and temporal variability was found in the equatorial zonal electric field. Figure 2d shows relative changes in the EEF from the time mean. It can be seen that the EEF underwent 6-day variations of ±40% that are out-of-phase for a 180° longitudinal separation. The amplitude varies in the range of 20–70% depending on the longitude. In a recent study, Yamazaki, Stolle, Matzka, and Alken (2018) reported that the EEJ intensity occasionally shows ∼6-day variations that have characteristics of a westward-propagating wave with ZW1. They attributed the EEJ variations to the quasi-6-day wave (Q6DW) that was simultaneously observed in the lower ther-

mosphere. The behavior of the EEJ presented in Figure 2a is similar to those reported by Yamazaki et al. (2018).

The Q6DW is a westward-propagating planetary wave with ZW1, which is occasionally observed in the middle atmosphere (e.g. Forbes & Zhang, 2017; Hirota & Hirooka, 1984; Pancheva, Mukhtarov, & Siskind, 2018; Riggin et al., 2006; Talaat, Yee, & Zhu, 2001, 2002; Wu, Hays, & Skinner, 1994). It is often regarded as the (1,1) Rossby normal mode, which is predicted by classical atmospheric wave theory (Forbes, 1995; Kasahara, 1976; Madden, 1979, 2007; Salby, 1984), for its zonal wavenumber, phase speed, and latitudinal structure. The Q6DW can be excited in the troposphere by heating due to moist convection (Miyoshi & Hirooka, 1999). Additionally, the wave can be excited/amplified in the middle atmosphere due to baroclinic/barotropic instability (Lieberman et al., 2003; H.-L. Liu et al., 2004; Meyer & Forbes, 1997). Zonal wind perturbations of the Q6DW are largest around the equator and can be up to a few tens of m/s at E-region heights, which is sufficient to cause detectable changes in dayside ionospheric electric fields and currents (Gan et al., 2016; Miyoshi, 1999; Pedatella, Liu, & Hagan, 2012). These electric field perturbations in the E-region ionosphere are transmitted to the F region along equipotential magnetic field lines, and affect the distribution of low-latitude F-region plasmas by modulating their $\mathbf{E}\times\mathbf{B}$ plasma drift motions. In this way, the Q6DW can affect the F-region plasma density, as first revealed in the 1990s by ionosonde measurements (e.g., Altadill & Laštovička, 1996; Apostolov, Alberca, & Altadill, 1994; Laštovička, 2006). More recent studies based on global TEC maps have established that the Q6DW effect on the plasma density is largest in the afternoon local time sector near the equatorial ionization anomaly crests ($\pm 20^\circ$ magnetic latitudes) (Gu et al., 2014; Gu, Ruan, et al., 2018; Qin et al., 2019; Yamazaki, 2018).

The 6-day variations can be seen in both electron density (Figures 2b and 2e) and top-side TEC (Figures 2c and 2f) at 20° magnetic latitude. (Figure S1 in Supporting Information shows the electron density variations at various latitudes.) The variations are consistent with those in the EEJ/EEF (Figures 2a and 2d), indicating electrodynamic coupling between the E- and F-region ionosphere. The response time of the F-region plasma density to a change in the E-region electric field is 2–4 hours (e.g., Stolle, Manoj, Lühr, Maus, & Alken, 2008; Venkatesh et al., 2015), which would not be visible in the figures. The relative change in the electron density is in the range of 20–40%, which is appreciably larger than that of TEC, 5–10%. This is not surprising as the amplitude of the

Q6DW decreases with altitude in the top-side ionosphere, as demonstrated by Gu, Ruan, et al. (2018).

The plasma density and TEC data from the ascending parts of the Swarm B orbit (02:00–23:00 MLT) were also examined, but the 6-day variations were not as evident as the results derived from the descending orbits. Similarly, the ionospheric data (EEJ, electron density, and TEC) from Swarm A, which was flying around 02:00–05:00 MLT (descending orbits) and 14:00–17:00 MLT (ascending orbits), did not show strong 6-day variations. The electron density variations from Swarm B (ascending) and Swarm A (ascending and descending) are presented in Supporting Information (Figure S2). The different behavior of 6-day variations in different Swarm datasets reflects the fact that the ionospheric response to the Q6DW depends on MLT and height, as well as on magnetic latitude (Gu, Ruan, et al., 2018). Further studies are required to determine the three dimensional structure of the 6-day ionospheric variations during this event.

Previous studies found a significant contribution of the semidiurnal lunar tide to ionospheric variability during NH SSWs (e.g., Park et al., 2012), but it is not known whether the lunar tide plays an equally important role during SH SSWs. The semidiurnal lunar variations in the EEJ intensity derived from the Swarm A and B data during 5 September–5 October 2019 are presented in Supporting Information (Figure S3). It is found that the amplitude of the EEJ semidiurnal lunar variation is 17.7±2.1 mA/m for Swarm A (14:00–17:00 MLT) and 16.6±2.8 mA/m for Swarm B (11:00–14:00 MLT), which is greater than the climatological value of 9.0±0.4 mA/m as reported by Yamazaki et al. (2017) for September daytime (08:00–16:00 local solar time) conditions. The phase, which is defined as the lunar time of maximum, is 10.2±0.2 h for Swarm A and 10.0±0.4 h for Swarm B, which is in good agreement with the climatological value of 10.0±0.1 h. Despite the significant enhancement, the lunar variation accounts for only a small part of the observed EEJ variability (compare Figures 2a and S3). The relative amplitude of the semidiurnal lunar variation in the top-side electron density is 9.9±0.7% for Swarm A and 11.1±0.1% for Swarm B (also shown in Figure S3). Again, these variations are smaller than the 6-day variations observed during the same period (Figure 2e).

It is noted that since Swarm slowly precesses in local solar time, it is not possible to resolve short-term variability of solar tides. Changes in upward-propagating solar tides can occur during SSWs due to changes in the zonal mean atmosphere (Jin et al., 2012;

Pedatella & Liu, 2013), tidal sources (Goncharenko, Coster, Plumb, & Domeisen, 2012), and tidal interaction with PWs (H.-L. Liu, Wang, Richmond, & Roble, 2010; Maute, Hagan, Richmond, & Roble, 2014). Possible changes in solar tides during the September 2019 SSW remain to be investigated.

2.3 Q6DW in the middle atmosphere

Traveling PWs in the middle atmosphere are examined using the GPH data from Aura/MLS. The analysis method was described in detail in the previous work (Yamazaki & Matthias, 2019), and thus is only briefly summarized here. The amplitude A and phase ϕ of waves with period τ were derived by fitting the following formula to the data at a given latitude and height:

$$\sum_{s=-4}^{4} A_s \cos\left[2\pi\left(\frac{t}{\tau} + s\lambda\right) - \phi_s\right], \tag{1}$$

where t is the universal time, λ is the longitude, and s is the zonal wavenumber. Eastward- and westward-propagating waves correspond to $s<0$ and $s>0$, respectively. The data were analyzed for each day using a time window that is 3 times the wave period. The 1-σ error in the amplitude is typically below 0.05 km.

Figures 3a and 3b show the amplitudes for the westward- and eastward-propagating waves with ZW1 at 45°S in the lower thermosphere at ∼97 km. Enhanced wave activity can be seen in the westward-propagating component (Figure 3a) with period 4–7d during September 2019, which can be identified as the Q6DW. It is consistent with the appearance of 6-day variations in the ionosphere (Figures 2a–2c). Such enhanced wave activity is not present in the eastward-propagating ZW1 component (Figure 3b), or other components with higher zonal wavenumbers (not shown here). Although studies have found that the amplitude of the Q6DW in the middle atmosphere is greatest during equinoctial months (Forbes & Zhang, 2017; Qin et al., 2019; Yamazaki, 2018), the wave enhancement in September 2019 was exceptional, with the maximum amplitude larger than 0.4 km in the lower thermosphere, which is much larger than the climatological amplitude (0.15 km) or amplitudes recorded during other individual years during 2004–2018 (Figure 3d). Thus, the large-amplitude Q6DW observed in September 2019 cannot be explained merely as a seasonal effect.

The latitude and height structures of the 6-day wave during 10–30 September 2019 are presented in Figure 3c. The amplitude and phase were derived at wave period of ex-

actly 6.0 days, so that the phases calculated at different heights and latitudes can be compared. In the mesosphere and lower thermosphere (above 50 km), the amplitude structure is symmetric about the equator with peaks at approximately ±45° latitudes, and the phase tends to be horizontally uniform with downward phase progression. These features are in conformity with the theoretically expected Q6DW in the presence of the mean winds and dissipation (e.g., Salby, 1981a, 1981b). Below 50 km, the phase progression is poleward as well as downward, especially in the SH, indicating equatorward and upward energy propagation from the high latitude region. Using reanalysis data, Gan, Oberheide, and Pedatella (2018) demonstrated how the Q6DW generated in the SH high latitude can propagate into the NH, growing to be a global mode in the mesosphere and lower thermosphere under September equinox conditions.

In Figure 3c, there is a region of locally enhanced amplitudes at 70–80°S and 20–50 km altitude, which can be regarded as a source of the large-amplitude Q6DW observed above. The amplification of the Q6DW from the seasonal background in this region is depicted in Figure 3e. Enhanced wave activity is observed in the same region over a wide range of wavenumbers (s from -3 to 3) and periods (τ=3–20d) (not shown here). A possible explanation for the wave amplification is baroclinic/barotropic instability (Gan et al., 2018; Lieberman et al., 2003; H.-L. Liu et al., 2004; Meyer & Forbes, 1997), in which waves can rapidly grow by extracting energy from the unstable mean flow. Figure 3f shows that the wave amplification in the polar middle atmosphere is not uncommon around this time of year, but in 2019, it took place at lower altitudes (∼30 km) than in other years (∼50 km).

Figures 3h–3j illustrates the development of the atmospheric instability. The areas highlighted by the light-yellow color indicate the regions where the necessary condition for barotropic/baroclinic instability is met; that is, the meridional gradient of the quasi-geostrophic potential vorticity is negative (e.g., H.-L. Liu et al., 2004). It can be seen that unstable regions are formed mainly around the edge of the polar vortex due to the strong vertical and horizontal shear in the zonal wind. As the westward mean flow descends to lower layers, the unstable regions at high latitudes (70–80°S) also move down, and hence exciting/amplifying waves at lower altitudes compared to other years. As these waves propagate equatorward and upward, the amplitude at 45°S is greater than other years above ∼40 km (Figure 3g). As numerically demonstrated by Salby (1981b), the vertical growth of amplitude is enhanced where the zonal mean zonal wind is weak and

eastward relative to the phase speed of the wave. The westward phase speed of the Q6DW is ∼55 m/s at 45°S and ∼13 m/s at 80°S. Thus, the reduced eastward mean flow and the weak wind reversal during the SSW (Figures 3h–3j) provide favorable conditions for the vertical propagation of the Q6DW. Interactions of the Q6DW with tides and gravity waves could also affect the vertical structure of the Q6DW (e.g., Forbes, Zhang, Maute, & Hagan, 2018; Meyer, 1999). A better understanding of the Q6DW propagation in the mesosphere and lower thermopshere during the September 2019 SSW would benefit from a more comprehensive analysis of dynamic fields from an atmospheric reanalysis or general circulation model.

For the NH, possible influence of SSWs on the vertical propagation of traveling planetary waves in the middle atmosphere has been discussed in a number of studies (e.g., Gu, Dou, Pancheva, Yi, & Chen, 2018; Hirooka & Hirota, 1985; Matthias, Hoffmann, Rapp, & Baumgarten, 2012; Pancheva et al., 2008; Sassi, Garcia, & Hoppel, 2012; Yamazaki & Matthias, 2019). In some cases, a strong Q6DW was observed during an SSW (e.g., Gong et al., 2018; Pancheva et al., 2018) but in general, there is no one-to-one correspondence between the occurrence of SSW and Q6DW enhancement in the NH (Yamazaki & Matthias, 2019). Modeling studies also found enhanced Q6DW activity following some SSWs, which has been attributed to barotropic/baroclinic instability in the NH high latitude (Chandran, Garcia, Collins, & Chang, 2013; Tomikawa et al., 2012). For the SH, studies are few because of infrequent occurrence of SSWs. Dowdy et al. (2004) and Espy, Hibbins, Riggin, and Fritts (2005) observed a westward-propagating planetary wave with ZW1 and period around 14d at 70–100 km altitude during the September 2002 Antarctic SSW. The present study finds a strong response of the Q6DW in the mesosphere and lower thermosphere during the September 2019 Antarctic SSW. It is possible that the response of traveling planetary waves to Antarctic SSWs varies from event to event. More studies are needed to clarify this point.

3 Summary and Conclusions

An SSW occurred in the Southern Hemisphere in September 2019. Although it was a minor warming, it involved an exceptionally strong wave-1 planetary wave and a large polar temperature enhancement by 50.8 K/week. The event also took place under solar minimum conditions, which is preferable for studying the ionospheric response. Ear-

lier studies focused on the effect of Northern-Hemisphere SSWs on the ionosphere, and few studies investigated Southern-Hemisphere cases.

The analysis of ionospheric data from ESA's Swarm mission during the September 2019 SSW reveals prominent 6-day variations in the dayside low-latitude region, including 20–70% variations in the equatorial zonal electric field, 20–40% variations in the top-side electron density, and 5–10% variations in the top-side total electron content. These variations are attributed to the Q6DW simultaneously observed in the middle atmosphere. Evidence is also found for enhanced lunar tidal perturbations in the ionosphere, but their amplitudes are relatively small (e.g., less than 15% in the top-side electron density).

The amplitude of the Q6DW in the lower thermosphere is more than 0.4 km in geopotential height, which is found to be the largest observed by Aura/MLS in the Southern Hemisphere since August 2004, and thus cannot be explained merely as a seasonal effect. The latitudinal and vertical structures of the Q6DW suggest that the waves are excited/amplified in the polar region at 30–40 km altitude, where the atmosphere is unstable due to strong vertical shear in the zonal wind connected with planetary-wave breaking. As the Q6DW grows in the vertical, the wave attains large amplitudes in the lower thermosphere, which drives ionospheric variability.

These results suggest that a Southern-Hemisphere SSW can lead to ionospheric variability by altering middle atmosphere dynamics and propagation characteristics of large-scale waves from the middle atmosphere to the upper atmosphere.

Acknowledgments

We thank the NASA Goddard Earth Sciences (GES) Data and Information Services Center (DISC) (https://disc.gsfc.nasa.gov/) for making the Aura/MLS geopotential height data and MERRA-2 data available. We also thank the European Space Agency (ESA) for providing the Swarm data (http://earth.esa.int/swarm). The geomagnetic activity index Kp was provided by the GFZ German Research Centre for Geosciences (https://www.gfz-potsdam.de/en/kp-index/). The solar activity index $F_{10.7}$ was downloaded from the SPDF OMNIWeb database (https://omniweb.gsfc.nasa.gov). This work was supported in part by ESA through contract 4000126709/19/NL/IS "VERA" and by the Deutsche Forschungsgemeinschaft (DFG) grant YA-574-3-1.

References

Alken, P., Maus, S., Chulliat, A., Vigneron, P., Sirol, O., & Hulot, G. (2015). Swarm equatorial electric field chain: first results. *Geophysical Research Letters*, *42*(3), 673–680.

Alken, P., Maus, S., Vigneron, P., Sirol, O., & Hulot, G. (2013). Swarm scarf equatorial electric field inversion chain. *Earth, Planets and Space*, *65*(11), 11.

Altadill, D., & Laštovička, J., Jan. (1996). Quasi-five-and ten-day oscillations in f0f2 and their possible connection with oscillations at lower ionospheric heights. *Annals of Geophysics*, *39*(4).

Andrews, D. G., Leovy, C. B., & Holton, J. R. (1987). *Middle atmosphere dynamics* (Vol. 40). Academic press.

Apostolov, E. M., Alberca, L., & Altadill, D. (1994). Solar cycle and seasonal behaviour of quasi two and rive day oscillations in the time variations of foF2. *Annals of Geophysics*, *37*(2).

Baldwin, M., Hirooka, T., O'Neill, A., & Yoden, S. (2003). Major stratospheric warming in the southern hemisphere in 2002: Dynamical aspects of the ozone hole split. *SPARC newsletter*, *20*, 24–26.

Buchert, S., Zangerl, F., Sust, M., André, M., Eriksson, A., Wahlund, J.-E., & Opgenoorth, H. (2015). Swarm observations of equatorial electron densities and topside gps track losses. *Geophysical Research Letters*, *42*(7), 2088–2092.

Butler, A. H., Seidel, D. J., Hardiman, S. C., Butchart, N., Birner, T., & Match, A. (2015). Defining sudden stratospheric warmings. *Bulletin of the American Meteorological Society*, *96*(11), 1913–1928.

Cámara, A. d. l., Albers, J. R., Birner, T., Garcia, R. R., Hitchcock, P., Kinnison, D. E., & Smith, A. K. (2017). Sensitivity of sudden stratospheric warmings to previous stratospheric conditions. *Journal of the Atmospheric Sciences*, *74*(9), 2857–2877.

Chandran, A., Collins, R., & Harvey, V. (2014). Stratosphere-mesosphere coupling during stratospheric sudden warming events. *Advances in Space Research*, *53*(9), 1265–1289.

Chandran, A., Garcia, R., Collins, R., & Chang, L. (2013). Secondary planetary waves in the middle and upper atmosphere following the stratospheric sudden warming event of January 2012. *Geophysical Research Letters*, *40*(9),

1861–1867.

Charlton, A. J., & Polvani, L. M. (2007). A new look at stratospheric sudden warmings. Part I: Climatology and modeling benchmarks. *Journal of Climate*, *20*(3), 449–469.

Chau, J., Aponte, N., Cabassa, E., Sulzer, M., Goncharenko, L. P., & González, S. (2010). Quiet time ionospheric variability over arecibo during sudden stratospheric warming events. *Journal of Geophysical Research: Space Physics*, *115*(A9).

Chau, J., Goncharenko, L. P., Fejer, B. G., & Liu, H.-L. (2012). Equatorial and low latitude ionospheric effects during sudden stratospheric warming events. *Space Science Reviews*, *168*(1-4), 385–417.

Chau, J., Hoffmann, P., Pedatella, N., Matthias, V., & Stober, G. (2015). Upper mesospheric lunar tides over middle and high latitudes during sudden stratospheric warming events. *Journal of Geophysical Research: Space Physics*, *120*(4), 3084–3096.

Dowdy, A. J., Vincent, R. A., Murphy, D. J., Tsutsumi, M., Riggin, D. M., & Jarvis, M. J. (2004). The large-scale dynamics of the mesosphere–lower thermosphere during the southern hemisphere stratospheric warming of 2002. *Geophysical Research Letters*, *31*(14).

Espy, P., Hibbins, R., Riggin, D., & Fritts, D. (2005). Mesospheric planetary waves over antarctica during 2002. *Geophysical Research Letters*, *32*(21).

Fang, T.-W., Fuller-Rowell, T., Akmaev, R., Wu, F., Wang, H., & Anderson, D. (2012). Longitudinal variation of ionospheric vertical drifts during the 2009 sudden stratospheric warming. *Journal of Geophysical Research: Space Physics*, *117*(A3).

Fang, T.-W., Fuller-Rowell, T., Wang, H., Akmaev, R., & Wu, F. (2014). Ionospheric response to sudden stratospheric warming events at low and high solar activity. *Journal of Geophysical Research: Space Physics*, *119*(9), 7858–7869.

Fejer, B. G., Olson, M., Chau, J., Stolle, C., Lühr, H., Goncharenko, L. P., ... Nagatsuma, T. (2010). Lunar-dependent equatorial ionospheric electrodynamic effects during sudden stratospheric warmings. *Journal of Geophysical Research: Space Physics*, *115*(A8).

Fejer, B. G., Tracy, B., Olson, M., & Chau, J. (2011). Enhanced lunar semidiurnal

equatorial vertical plasma drifts during sudden stratospheric warmings. *Geophysical Research Letters*, *38*(21).

Forbes, J. M. (1995). Tidal and planetary waves. *The upper mesosphere and lower thermosphere: a review of experiment and theory*, *87*, 67–87.

Forbes, J. M., & Zhang, X. (2012). Lunar tide amplification during the January 2009 stratosphere warming event: Observations and theory. *Journal of Geophysical Research: Space Physics*, *117*(A12).

Forbes, J. M., & Zhang, X. (2017). The quasi-6 day wave and its interactions with solar tides. *Journal of Geophysical Research: Space Physics*, *122*(4), 4764–4776.

Forbes, J. M., Zhang, X., Maute, A., & Hagan, M. E. (2018). Zonally symmetric oscillations of the thermosphere at planetary wave periods. *Journal of Geophysical Research: Space Physics*, *123*(5), 4110–4128.

Friis-Christensen, E., Lühr, H., & Hulot, G. (2006). Swarm: A constellation to study the earth's magnetic field. *Earth, planets and space*, *58*(4), 351–358.

Friis-Christensen, E., Lühr, H., Knudsen, D., & Haagmans, R. (2008). Swarm–an earth observation mission investigating geospace. *Advances in Space Research*, *41*(1), 210–216.

Fuller-Rowell, T., Wang, H., Akmaev, R., Wu, F., Fang, T.-W., Iredell, M., & Richmond, A. (2011). Forecasting the dynamic and electrodynamic response to the January 2009 sudden stratospheric warming. *Geophysical Research Letters*, *38*(13).

Gan, Q., Oberheide, J., & Pedatella, N. M. (2018). Sources, sinks, and propagation characteristics of the quasi 6-day wave and its impact on the residual mean circulation. *Journal of Geophysical Research: Atmospheres*, *123*(17), 9152–9170.

Gan, Q., Wang, W., Yue, J., Liu, H., Chang, L. C., Zhang, S., ... Du, J. (2016). Numerical simulation of the 6 day wave effects on the ionosphere: Dynamo modulation. *Journal of Geophysical Research: Space Physics*, *121*(10), 10–103.

Gelaro, R., McCarty, W., Suárez, M. J., Todling, R., Molod, A., Takacs, L., ... others (2017). The modern-era retrospective analysis for research and applications, version 2 (MERRA-2). *Journal of Climate*, *30*(14), 5419–5454.

Goncharenko, L. P., Chau, J., Liu, H.-L., & Coster, A. (2010). Unexpected connec-

tions between the stratosphere and ionosphere. *Geophysical Research Letters*, *37*(10).

Goncharenko, L. P., Coster, A., Chau, J., & Valladares, C. (2010). Impact of sudden stratospheric warmings on equatorial ionization anomaly. *Journal of Geophysical Research: Space Physics*, *115*(A10).

Goncharenko, L. P., Coster, A., Plumb, R. A., & Domeisen, D. I. (2012). The potential role of stratospheric ozone in the stratosphere-ionosphere coupling during stratospheric warmings. *Geophysical Research Letters*, *39*(8).

Gong, Y., Li, C., Ma, Z., Zhang, S., Zhou, Q., Huang, C., ... Ning, B. (2018). Study of the quasi-5-day wave in the mlt region by a meteor radar chain. *Journal of Geophysical Research: Atmospheres*, *123*(17), 9474–9487.

Gu, S.-Y., Dou, X., Pancheva, D., Yi, W., & Chen, T. (2018). Investigation of the abnormal quasi 2-day wave activities during the sudden stratospheric warming period of January 2006. *Journal of Geophysical Research: Space Physics*, *123*(7), 6031–6041.

Gu, S.-Y., Liu, H.-L., Li, T., Dou, X., Wu, Q., & Russell III, J. M. (2014). Observation of the neutral-ion coupling through 6 day planetary wave. *Journal of Geophysical Research: Space Physics*, *119*(12), 10–376.

Gu, S.-Y., Ruan, H., Yang, C.-Y., Gan, Q., Dou, X., & Wang, N. (2018). The morphology of the 6-day wave in both the neutral atmosphere and f region ionosphere under solar minimum conditions. *Journal of Geophysical Research: Space Physics*, *123*(5), 4232–4240.

Hirooka, T., & Hirota, I. (1985). Normal mode rossby waves observed in the upper stratosphere. Part II: Second antisymmetric and symmetric modes of zonal wavenumbers 1 and 2. *Journal of the atmospheric sciences*, *42*(6), 536–548.

Hirota, I., & Hirooka, T. (1984). Normal mode rossby waves observed in the upper stratosphere. Part I: First symmetric modes of zonal wavenumbers 1 and 2. *Journal of the atmospheric sciences*, *41*(8), 1253–1267.

Jin, H., Miyoshi, Y., Pancheva, D., Mukhtarov, P., Fujiwara, H., & Shinagawa, H. (2012). Response of migrating tides to the stratospheric sudden warming in 2009 and their effects on the ionosphere studied by a whole atmosphere-ionosphere model GAIA with COSMIC and TIMED/SABER observations. *Journal of Geophysical Research: Space Physics*, *117*(A10).

Kasahara, A. (1976). Normal modes of ultralong waves in the atmosphere. *Monthly Weather Review*, *104*(6), 669–690.

Krüger, K., Naujokat, B., & Labitzke, K. (2005). The unusual midwinter warming in the southern hemisphere stratosphere 2002: A comparison to northern hemisphere phenomena. *Journal of the atmospheric sciences*, *62*(3), 603–613.

Labitzke, K., & Van Loon, H. (1999). *The stratosphere: phenomena, history, and relevance*. Springer Science & Business Media.

Laštovička, J. (2006). Forcing of the ionosphere by waves from below. *Journal of Atmospheric and Solar-Terrestrial Physics*, *68*(3-5), 479–497.

Lieberman, R., Riggin, D., Franke, S., Manson, A., Meek, C., Nakamura, T., ... Reid, I. (2003). The 6.5-day wave in the mesosphere and lower thermosphere: Evidence for baroclinic/barotropic instability. *Journal of Geophysical Research: Atmospheres*, *108*(D20).

Limpasuvan, V., Thompson, D. W., & Hartmann, D. L. (2004). The life cycle of the northern hemisphere sudden stratospheric warmings. *Journal of Climate*, *17*(13), 2584–2596.

Lin, J.-T., Lin, C., Lin, C., Pedatella, N. M., Rajesh, P., Matsuo, T., & Liu, J. (2019). Revisiting the modulations of ionospheric solar and lunar migrating tides during the 2009 stratospheric sudden warming by using global ionosphere specification. *Space Weather*, *17*(5), 767–777.

Liu, H., Yamamoto, M., Tulasi Ram, S., Tsugawa, T., Otsuka, Y., Stolle, C., ... Nagatsuma, T. (2011). Equatorial electrodynamics and neutral background in the asian sector during the 2009 stratospheric sudden warming. *Journal of Geophysical Research: Space Physics*, *116*(A8).

Liu, H.-L., & Richmond, A. (2013). Attribution of ionospheric vertical plasma drift perturbations to large-scale waves and the dependence on solar activity. *Journal of Geophysical Research: Space Physics*, *118*(5), 2452–2465.

Liu, H.-L., Talaat, E., Roble, R., Lieberman, R., Riggin, D., & Yee, J.-H. (2004). The 6.5-day wave and its seasonal variability in the middle and upper atmosphere. *Journal of Geophysical Research: Atmospheres*, *109*(D21).

Liu, H.-L., Wang, W., Richmond, A., & Roble, R. (2010). Ionospheric variability due to planetary waves and tides for solar minimum conditions. *Journal of Geophysical Research: Space Physics*, *115*(A6).

Liu, J., Zhang, D.-H., Hao, Y.-Q., & Xiao, Z. (2019). The comparison of lunar tidal characteristics in the low-latitudinal ionosphere between east asian and american sectors during stratospheric sudden warming events: 2009-2018. *Journal of Geophysical Research: Space Physics*.

Madden, R. A. (1979). Observations of large-scale traveling rossby waves. *Reviews of Geophysics*, *17*(8), 1935–1949.

Madden, R. A. (2007). Large-scale, free rossby waves in the atmosphere—an update. *Tellus A: Dynamic Meteorology and Oceanography*, *59*(5), 571–590.

Matsuno, T. (1971). A dynamical model of the stratospheric sudden warming. *Journal of the Atmospheric Sciences*, *28*(8), 1479–1494.

Matthias, V., & Ern, M. (2018). On the origin of the mesospheric quasi-stationary planetary waves in the unusual arctic winter 2015/2016. *Atmospheric Chemistry and Physics*, *18*(7), 4803–4815.

Matthias, V., Hoffmann, P., Rapp, M., & Baumgarten, G. (2012). Composite analysis of the temporal development of waves in the polar mlt region during stratospheric warmings. *Journal of Atmospheric and Solar-Terrestrial Physics*, *90*, 86–96.

Maute, A., Hagan, M., Richmond, A., & Roble, R. (2014). TIME-GCM study of the ionospheric equatorial vertical drift changes during the 2006 stratospheric sudden warming. *Journal of Geophysical Research: Space Physics*, *119*(2), 1287–1305.

McInturff, R. M. (1978). *Stratospheric warmings: Synoptic, dynamic and general-circulation aspects* (Tech. Rep. No. Ref. Publ. 1017). Suitland, Md.. (available online at https://ntrs.nasa.gov/archive/nasa/casi.ntrs.nasa.gov/19780010687.pdf)

McIntyre, M. E. (1982). How well do we understand the dynamics of stratospheric warmings? *Journal of the Meteorological Society of Japan. Ser. II*, *60*(1), 37–65.

Meyer, C. K. (1999). Gravity wave interactions with mesospheric planetary waves: A mechanism for penetration into the thermosphere-ionosphere system. *Journal of Geophysical Research: Space Physics*, *104*(A12), 28181–28196.

Meyer, C. K., & Forbes, J. M. (1997). A 6.5-day westward propagating planetary wave: Origin and characteristics. *Journal of Geophysical Research: Atmo-*

spheres, *102*(D22), 26173–26178.

Miyoshi, Y. (1999). Numerical simulation of the 5-day and 16-day waves in the mesopause region. *Earth, planets and space*, *51*(7-8), 763–772.

Miyoshi, Y., & Hirooka, T. (1999). A numerical experiment of excitation of the 5-day wave by a GCM. *Journal of the atmospheric sciences*, *56*(11), 1698–1707.

Nayak, C., & Yiğit, E. (2019). Variation of small-scale gravity wave activity in the ionosphere during the major sudden stratospheric warming event of 2009. *Journal of Geophysical Research: Space Physics*, *124*(1), 470–488.

Olson, M., Fejer, B., Stolle, C., Lühr, H., & Chau, J. (2013). Equatorial ionospheric electrodynamic perturbations during southern hemisphere stratospheric warming events. *Journal of Geophysical Research: Space Physics*, *118*(3), 1190–1195.

Oyama, K.-I., Jhou, J., Lin, J., Lin, C., Liu, H., & Yumoto, K. (2014). Ionospheric response to 2009 sudden stratospheric warming in the northern hemisphere. *Journal of Geophysical Research: Space Physics*, *119*(12), 10–260.

Pancheva, D., & Mukhtarov, P. (2011). Stratospheric warmings: The atmosphere–ionosphere coupling paradigm. *Journal of Atmospheric and Solar-Terrestrial Physics*, *73*(13), 1697–1702.

Pancheva, D., Mukhtarov, P., Mitchell, N., Merzlyakov, E., Smith, A., Andonov, B., ... others (2008). Planetary waves in coupling the stratosphere and mesosphere during the major stratospheric warming in 2003/2004. *Journal of Geophysical Research: Atmospheres*, *113*(D12).

Pancheva, D., Mukhtarov, P., & Siskind, D. E. (2018). The quasi-6-day waves in nogaps-alpha forecast model and their climatology in mls/aura measurements (2005–2014). *Journal of Atmospheric and Solar-Terrestrial Physics*, *181*, 19–37.

Park, J., Lühr, H., Kervalishvili, G., Rauberg, J., Stolle, C., Kwak, Y.-S., & Lee, W. K. (2017). Morphology of high-latitude plasma density perturbations as deduced from the total electron content measurements onboard the swarm constellation. *Journal of Geophysical Research: Space Physics*, *122*(1), 1338–1359.

Park, J., Lühr, H., Kunze, M., Fejer, B. G., & Min, K. W. (2012). Effect of sudden stratospheric warming on lunar tidal modulation of the equatorial electrojet.

Journal of Geophysical Research: Space Physics, *117*(A3).

Patra, A., Pavan Chaitanya, P., Sripathi, S., & Alex, S. (2014). Ionospheric variability over indian low latitude linked with the 2009 sudden stratospheric warming. *Journal of Geophysical Research: Space Physics*, *119*(5), 4044–4061.

Pedatella, N., Chau, J., Schmidt, H., Goncharenko, L., Stolle, C., Hocke, K., ... Siddiqui, T. (2018). How sudden stratospheric warming affects the whole atmosphere. *Eos*, *99*, 35–38.

Pedatella, N., & Forbes, J. (2010). Evidence for stratosphere sudden warming-ionosphere coupling due to vertically propagating tides. *Geophysical Research Letters*, *37*(11).

Pedatella, N., & Liu, H.-L. (2013). The influence of atmospheric tide and planetary wave variability during sudden stratosphere warmings on the low latitude ionosphere. *Journal of Geophysical Research: Space Physics*, *118*(8), 5333–5347.

Pedatella, N., Liu, H.-L., & Hagan, M. (2012). Day-to-day migrating and nonmigrating tidal variability due to the six-day planetary wave. *Journal of Geophysical Research: Space Physics*, *117*(A6).

Pedatella, N., Liu, H.-L., Sassi, F., Lei, J., Chau, J., & Zhang, X. (2014). Ionosphere variability during the 2009 ssw: Influence of the lunar semidiurnal tide and mechanisms producing electron density variability. *Journal of Geophysical Research: Space Physics*, *119*(5), 3828–3843.

Pedatella, N., & Maute, A. (2015). Impact of the semidiurnal lunar tide on the midlatitude thermospheric wind and ionosphere during sudden stratosphere warmings. *Journal of Geophysical Research: Space Physics*, *120*(12), 10–740.

Qin, Y., Gu, S.-Y., Dou, X., Gong, Y., Chen, G., Zhang, S., & Wu, Q. (2019). Climatology of the quasi-6-day wave in the mesopause region and its modulations on total electron content during 2003–2017. *Journal of Geophysical Research: Space Physics*, *124*(1), 573–583.

Riggin, D. M., Liu, H.-L., Lieberman, R. S., Roble, R. G., Russell Iii, J. M., Mertens, C. J., ... others (2006). Observations of the 5-day wave in the mesosphere and lower thermosphere. *Journal of Atmospheric and Solar-Terrestrial Physics*, *68*(3-5), 323–339.

Rodrigues, F., Crowley, G., Azeem, S., & Heelis, R. (2011). C/nofs observations of the equatorial ionospheric electric field response to the 2009 major sudden

stratospheric warming event. *Journal of Geophysical Research: Space Physics*, *116*(A9).

Salby, M. L. (1981a). Rossby normal modes in nonuniform background configurations. Part II. equinox and solstice conditions. *Journal of the Atmospheric Sciences*, *38*(9), 1827–1840.

Salby, M. L. (1981b). Rossby normal modes in nonuniform background configurations. Part I: Simple fields. *Journal of the Atmospheric Sciences*, *38*(9), 1803–1826.

Salby, M. L. (1984). Survey of planetary-scale traveling waves: The state of theory and observations. *Reviews of Geophysics*, *22*(2), 209–236.

Sassi, F., Garcia, R., & Hoppel, K. (2012). Large-scale rossby normal modes during some recent northern hemisphere winters. *Journal of the Atmospheric Sciences*, *69*(3), 820–839.

Sassi, F., Liu, H.-L., Ma, J., & Garcia, R. R. (2013). The lower thermosphere during the northern hemisphere winter of 2009: A modeling study using high-altitude data assimilation products in WACCM-X. *Journal of Geophysical Research: Atmospheres*, *118*(16), 8954–8968.

Schwartz, M., Lambert, A., Manney, G., Read, W., Livesey, N., Froidevaux, L., ... others (2008). Validation of the aura microwave limb sounder temperature and geopotential height measurements. *Journal of Geophysical Research: Atmospheres*, *113*(D15).

Siddiqui, T. A., Maute, A., Pedatella, N., Yamazaki, Y., Lühr, H., & Stolle, C. (2018). On the variability of the semidiurnal solar and lunar tides of the equatorial electrojet during sudden stratospheric warmings. In *Annales geophysicae* (Vol. 36, pp. 1545–1562).

Siddiqui, T. A., Stolle, C., Lühr, H., & Matzka, J. (2015). On the relationship between weakening of the northern polar vortex and the lunar tidal amplification in the equatorial electrojet. *Journal of Geophysical Research: Space Physics*, *120*(11), 10006–10019.

Stening, R., Forbes, J., Hagan, M., & Richmond, A. (1997). Experiments with a lunar atmospheric tidal model. *Journal of Geophysical Research: Atmospheres*, *102*(D12), 13465–13471.

Stolle, C., Manoj, C., Lühr, H., Maus, S., & Alken, P. (2008). Estimating the day-

time equatorial ionization anomaly strength from electric field proxies. *Journal of Geophysical Research: Space Physics*, *113*(A9).

Talaat, E., Yee, J.-H., & Zhu, X. (2001). Observations of the 6.5-day wave in the mesosphere and lower thermosphere. *Journal of Geophysical Research: Atmospheres*, *106*(D18), 20715–20723.

Talaat, E., Yee, J.-H., & Zhu, X. (2002). The 6.5-day wave in the tropical stratosphere and mesosphere. *Journal of Geophysical Research: Atmospheres*, *107*(D12), ACL–1.

Tomikawa, Y., Sato, K., Watanabe, S., Kawatani, Y., Miyazaki, K., & Takahashi, M. (2012). Growth of planetary waves and the formation of an elevated stratopause after a major stratospheric sudden warming in a T213L256 GCM. *Journal of Geophysical Research: Atmospheres*, *117*(D16).

Venkatesh, K., Fagundes, P., Prasad, D. V., Denardini, C. M., De Abreu, A., De Jesus, R., & Gende, M. (2015). Day-to-day variability of equatorial electrojet and its role on the day-to-day characteristics of the equatorial ionization anomaly over the indian and brazilian sectors. *Journal of Geophysical Research: Space Physics*, *120*(10), 9117–9131.

Wang, H., Akmaev, R., Fang, T.-W., Fuller-Rowell, T., Wu, F., Maruyama, N., & Iredell, M. (2014). First forecast of a sudden stratospheric warming with a coupled whole-atmosphere/ionosphere model idea. *Journal of Geophysical Research: Space Physics*, *119*(3), 2079–2089.

Waters, J. W., Froidevaux, L., Harwood, R. S., Jarnot, R. F., Pickett, H. M., Read, W. G., ... others (2006). The earth observing system microwave limb sounder (eos mls) on the aura satellite. *IEEE Transactions on Geoscience and Remote Sensing*, *44*(5), 1075–1092.

Wu, D., Hays, P., & Skinner, W. (1994). Observations of the 5-day wave in the mesosphere and lower thermosphere. *Geophysical Research Letters*, *21*(24), 2733–2736.

Yadav, S., Pant, T. K., Choudhary, R., Vineeth, C., Sunda, S., Kumar, K., ... Mukherjee, S. (2017). Impact of sudden stratospheric warming of 2009 on the equatorial and low-latitude ionosphere of the indian longitudes: A case study. *Journal of Geophysical Research: Space Physics*, *122*(10), 10–486.

Yamazaki, Y. (2018). Quasi-6-day wave effects on the equatorial ionization anomaly

683 over a solar cycle. *Journal of Geophysical Research: Space Physics*, *123*(11),
684 9881–9892.
685 Yamazaki, Y., & Matthias, V. (2019). Large-amplitude quasi-10-day waves in
686 the middle atmosphere during final warmings. *Journal of Geophysical Re-*
687 *search: Atmospheres*, *124*(17-18), 9874-9892. Retrieved from `https://`
688 `agupubs.onlinelibrary.wiley.com/doi/abs/10.1029/2019JD030634` doi:
689 10.1029/2019JD030634
690 Yamazaki, Y., & Maute, A. (2017). Sq and eej—a review on the daily variation
691 of the geomagnetic field caused by ionospheric dynamo currents. *Space Science*
692 *Reviews*, *206*(1-4), 299–405.
693 Yamazaki, Y., Richmond, A., Maute, A., Liu, H.-L., Pedatella, N., & Sassi, F.
694 (2014). On the day-to-day variation of the equatorial electrojet during quiet
695 periods. *Journal of Geophysical Research: Space Physics*, *119*(8), 6966–6980.
696 Yamazaki, Y., Richmond, A., & Yumoto, K. (2012). Stratospheric warmings and the
697 geomagnetic lunar tide: 1958–2007. *Journal of Geophysical Research: Space*
698 *Physics*, *117*(A4).
699 Yamazaki, Y., Stolle, C., Matzka, J., & Alken, P. (2018). Quasi-6-day wave mod-
700 ulation of the equatorial electrojet. *Journal of Geophysical Research: Space*
701 *Physics*, *123*(5), 4094–4109.
702 Yamazaki, Y., Stolle, C., Matzka, J., Siddiqui, T. A., Lühr, H., & Alken, P. (2017).
703 Longitudinal variation of the lunar tide in the equatorial electrojet. *Journal of*
704 *Geophysical Research: Space Physics*, *122*(12), 12–445.
705 Yue, X., Schreiner, W. S., Lei, J., Rocken, C., Hunt, D. C., Kuo, Y.-H., & Wan, W.
706 (2010). Global ionospheric response observed by COSMIC satellites during
707 the January 2009 stratospheric sudden warming event. *Journal of Geophysical*
708 *Research: Space Physics*, *115*(A11).
709 Zhang, X., & Forbes, J. M. (2014). Lunar tide in the thermosphere and weakening of
710 the northern polar vortex. *Geophysical Research Letters*, *41*(23), 8201–8207.

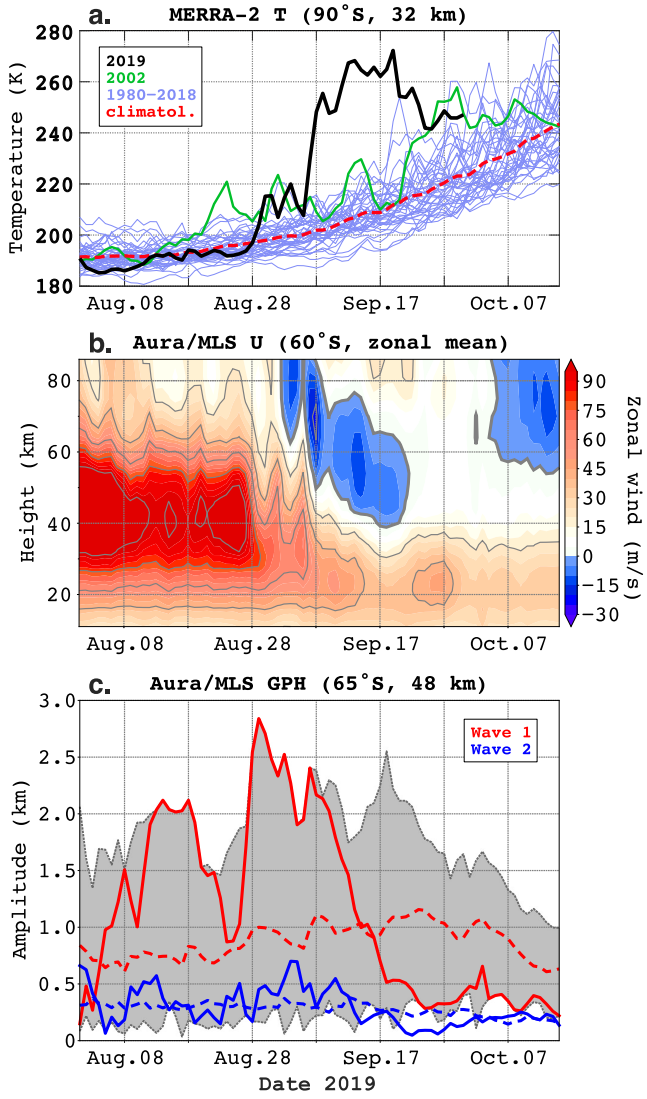

Figure 1. Overview of middle atmosphere dynamics during the September 2019 sudden stratospheric warming. (a) Stratospheric polar temperature at 10 hPa obtained from the MERRA-2 reanalysis. The thick black line represents the data for 2019, while the thin purple lines correspond to the data for other years during 1980–2018, among which the data for 2002 are highlighted by green for the occurrence of a major SSW. The red dashed line shows the climatological mean. (b) Zonal mean zonal wind at 60°S derived from the geopotential height (GPH) measurements by the Aura Microwave Limb Sounder (MLS) using the method described by Matthias and Ern (2018). (c) Amplitude of the planetary wave with Zonal Wavenumber (ZW) 1 and ZW2 at 65°S and 48 km altitude from the Aura/MLS GPH. The red and blue solid lines represent ZW1 and ZW2 waves, respectively. The climatological amplitudes of the ZW1 and ZW2 waves are indicated by the dashed lines with corresponding colors. The gray shaded area show the range between the maximum and minimum values of the amplitude of the ZW1 wave observed by Aura/MLS since August 2004.

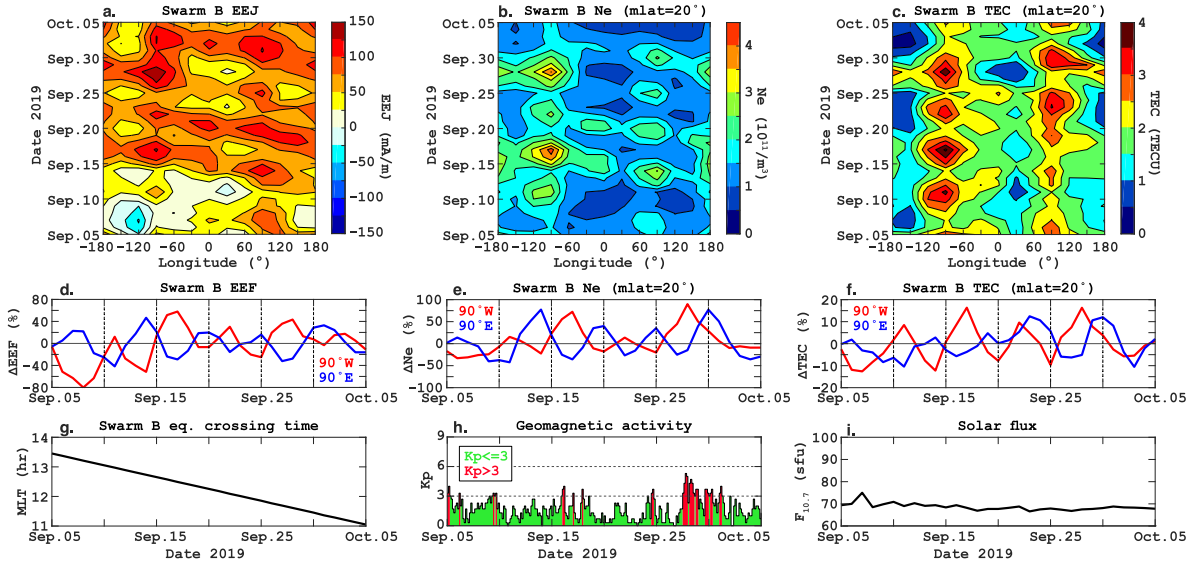

Figure 2. Overview of ionospheric variations during 5 September–5 October 2019. (a) Longitude versus time plot of the equatorial electrojet (EEJ) intensity derived from magnetic field measurements in the descending orbits of Swarm B. The data are smoothed using a 3-day and 50°-longitude window. (b) Same as (a) except for the electron density at 20° magnetic latitude. (c) Same as (a) except for the total electron content (TEC) at 20° magnetic latitude at the satellite altitude of ∼510 km. (d) Percent changes in the Swarm B zonal equatorial electric field (EEF) at ±90° longitudes with respect to the time mean at the corresponding longitudes. (e) Same as (d) except for the Swarm B electron density at 20° magnetic latitude. (f) Same as (d) except for the Swarm B TEC at 20° magnetic latitude. (g) Magnetic local time (MLT) at equatorial crossings for the descending orbits of Swarm B. (h) Geomagnetic activity index Kp. (i) Solar activity index $F_{10.7}$.

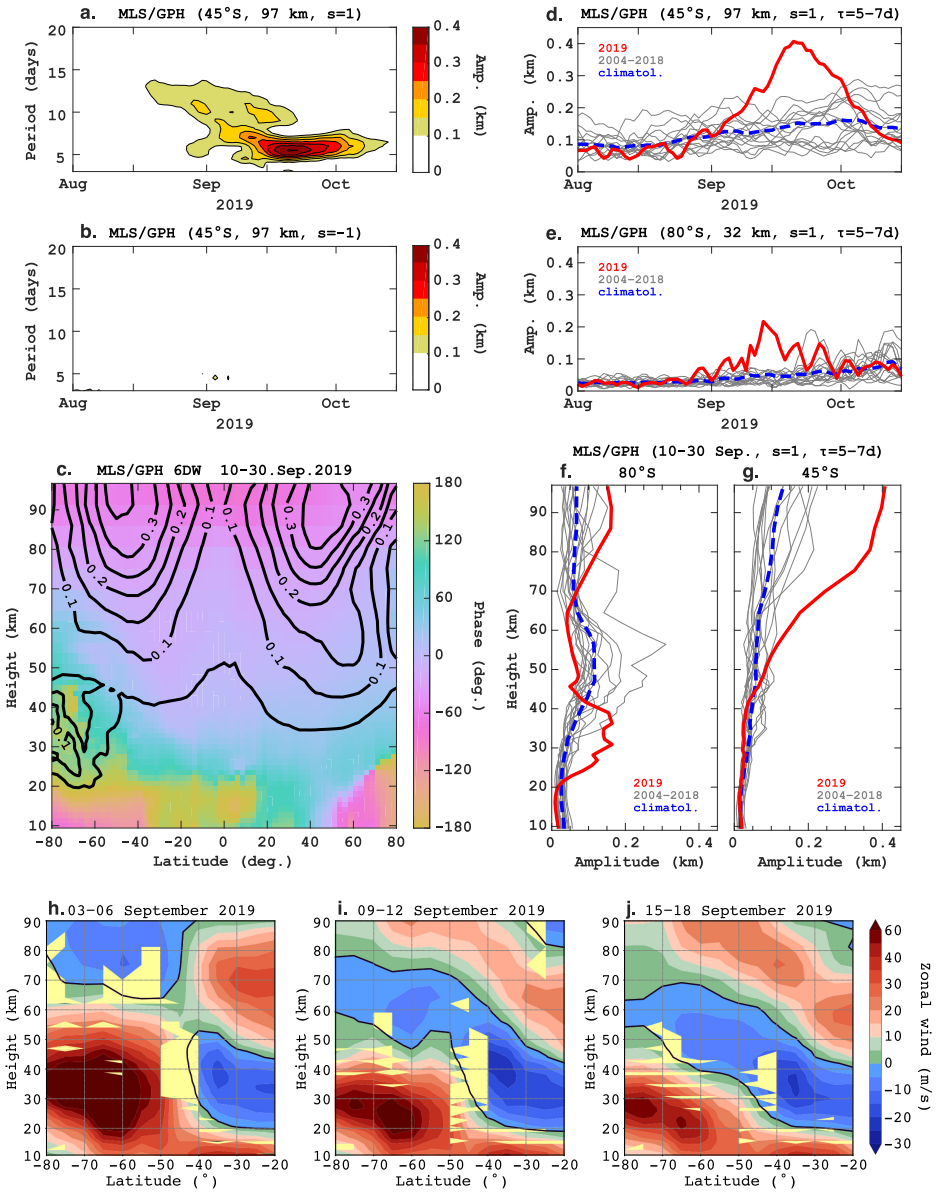

Figure 3. Overview of quasi-6-day wave (Q6DW) activity during the September 2019 SSW as derived from the geopotential height (GPH) measurements by the Aura Microwave Limb Sounder (MLS). (a) Amplitude of the westward-propagating Zonal Wavenumber (ZW) 1 waves at 45°S and 97 km altitude. (b) Same as (a) except for the eastward-propagating ZW1 waves. (c) Latitude versus height structures of the westward-propagating ZW1 wave with period 6.0d during 10–30 September 2019. The contour lines indicate the amplitude while the color represents the phase. (d) Amplitude of the Q6DW, defined here as the maximum amplitude of the westward-propagating ZW1 waves at periods 5–7d, at 45°S and 97 km altitude. (e) Same as (d) except at 80°S and 32 km altitude. (f) Vertical structure of the Q6DW at 80°S during 10–30 September 2019. (g) Same as (f) except at 45°S. (h–j) Latitude versus height structures of the zonal mean zonal wind. The areas highlighted by the light-yellow color indicate the regions where the meridional gradient of the quasi-geostrophic potential vorticity is negative, which is the necessary condition for barotropic/baroclinic instability.

Figure 1.

a. MERRA-2 T (90°S, 32 km)

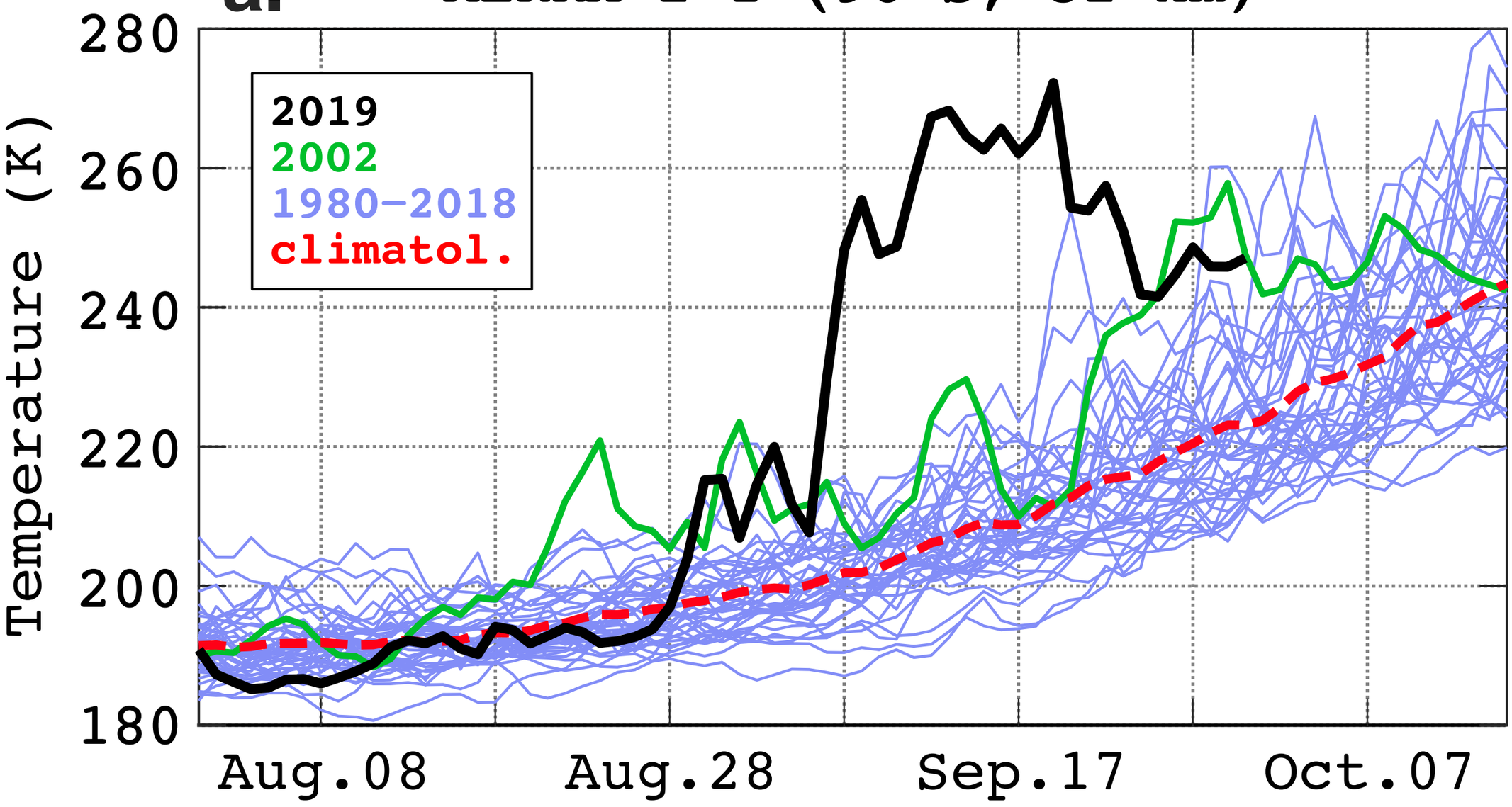

b. Aura/MLS U (60°S, zonal mean)

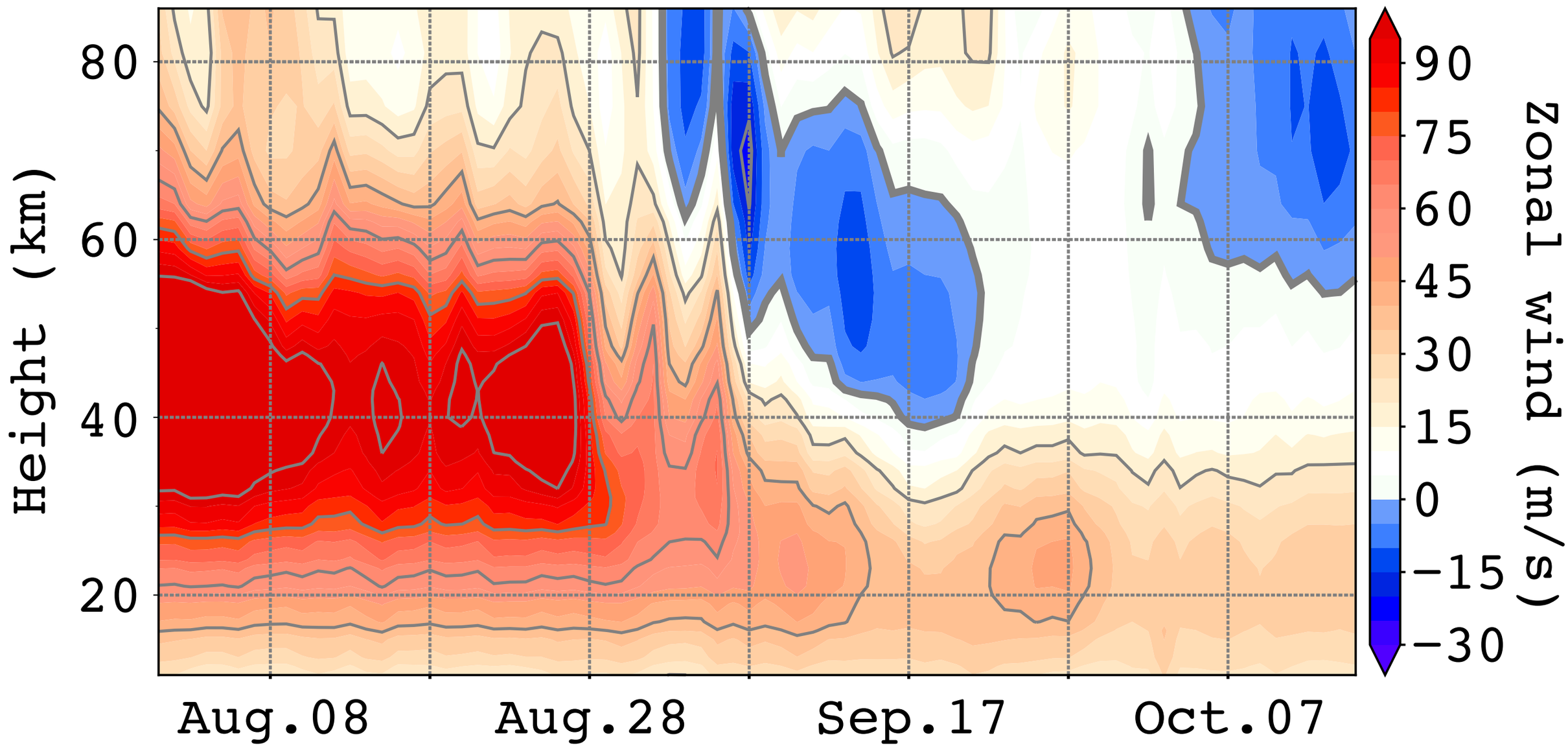

c. Aura/MLS GPH (65°S, 48 km)

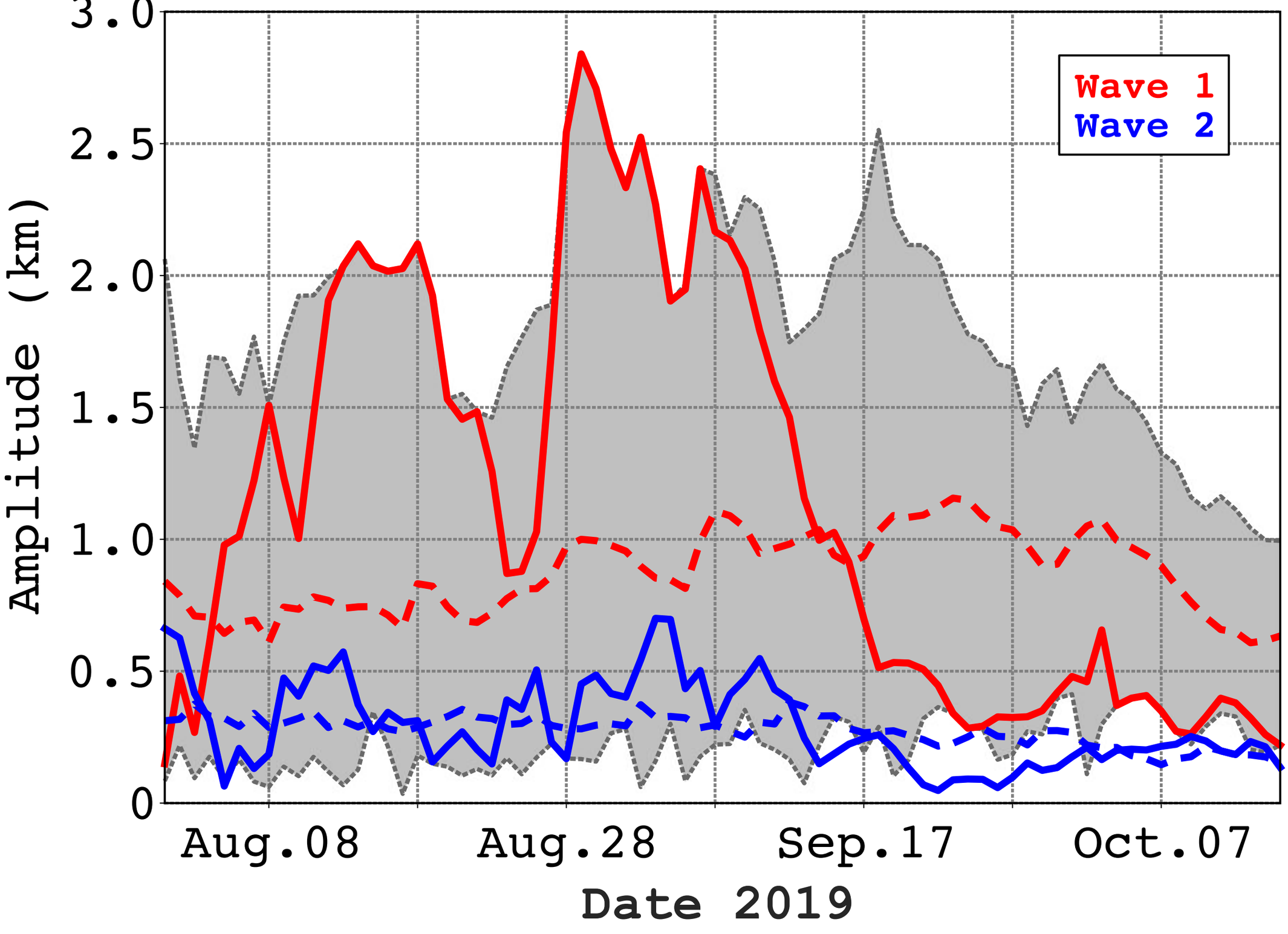

Figure 2.

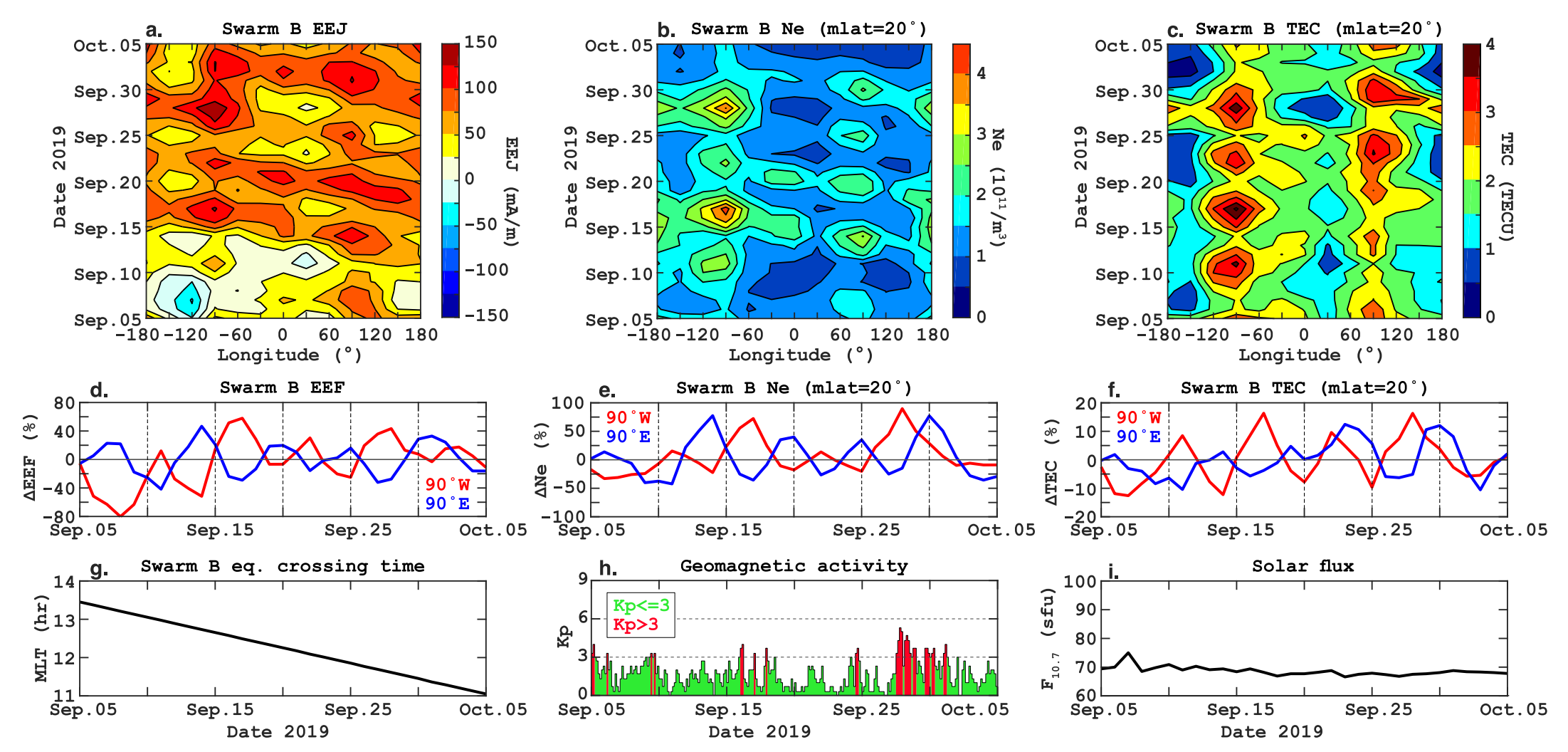
a. Swarm B EEJ
Oct.05
Sep.30
Sep.25
Sep.20
Sep.15
Sep.10
Sep.05
Date 2019
-180 -120 -60 0 60 120 180
Longitude (°)
150
100
50
0
-50
-100
-150
EEJ (mA/m)
b. Swarm B Ne (mlat=20°)
Ne (10^11/m^3)
c. Swarm B TEC (mlat=20°)
TEC (TECU)
d. Swarm B EEF
ΔEEF (%)
90°W
90°E
e. Swarm B Ne (mlat=20°)
ΔNe (%)
f. Swarm B TEC (mlat=20°)
ΔTEC (%)
g. Swarm B eq. crossing time
MLT (hr)
Sep.05
Sep.15
Sep.25
Oct.05
Date 2019
h. Geomagnetic activity
Kp
Kp<=3
Kp>3
i. Solar flux
F10.7 (sfu)

Figure 3.

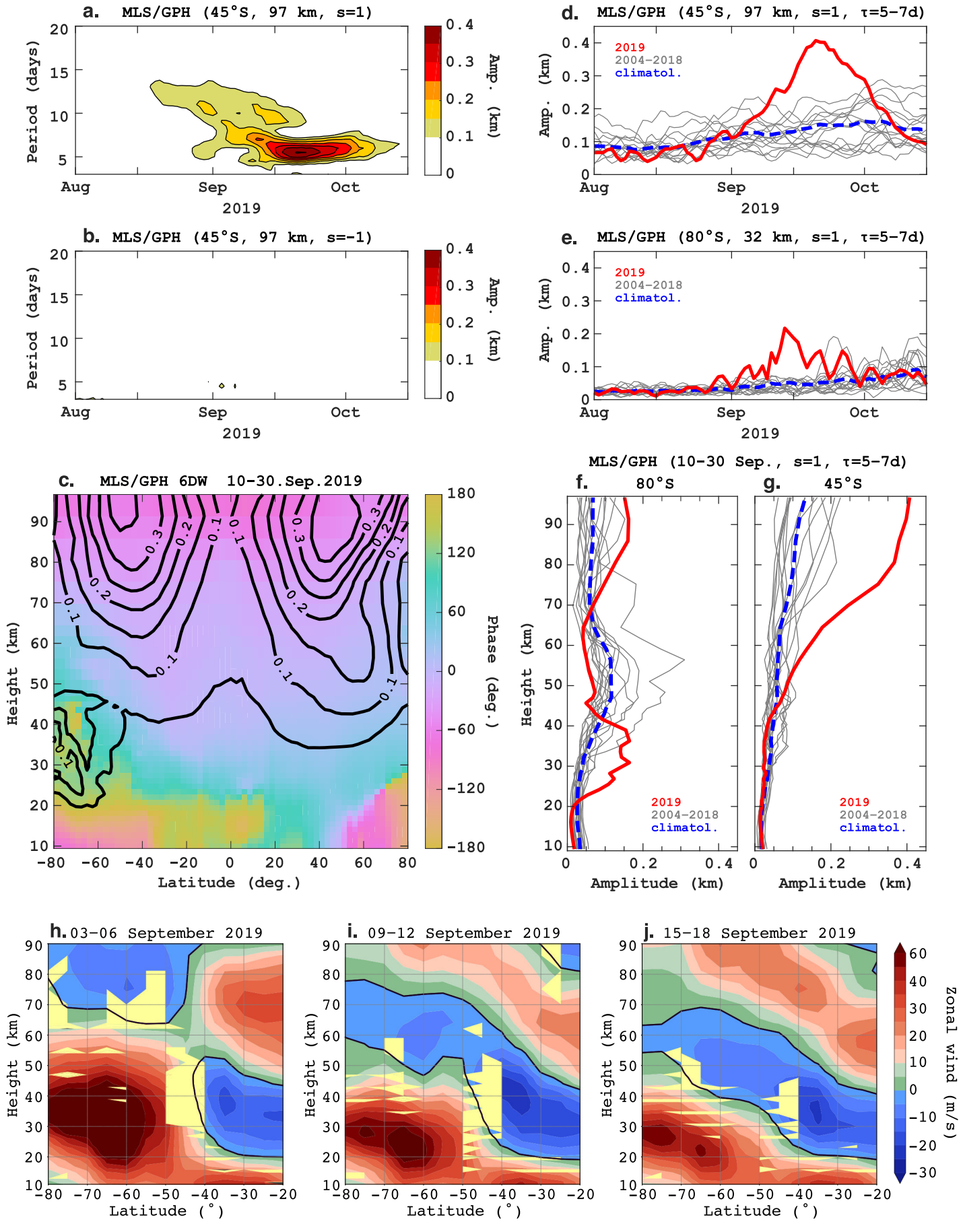
a. MLS/GPH (45°S, 97 km, s=1)
Period (days)
Amp. (km)
Aug
Sep
Oct
2019
b. MLS/GPH (45°S, 97 km, s=-1)
d. MLS/GPH (45°S, 97 km, s=1, τ=5-7d)
2019
2004-2018
climatol.
e. MLS/GPH (80°S, 32 km, s=1, τ=5-7d)
c. MLS/GPH 6DW 10-30.Sep.2019
Height (km)
Phase (deg.)
Latitude (deg.)
MLS/GPH (10-30 Sep., s=1, τ=5-7d)
f. 80°S
g. 45°S
Amplitude (km)
h. 03-06 September 2019
i. 09-12 September 2019
j. 15-18 September 2019
Latitude (°)
Zonal wind (m/s)